Astroparticle Physics 42 (2013) 1–6

Contents lists available at SciVerse ScienceDirect

Astroparticle Physics

journal homepage: www.elsevier.com/locate/astropart

Measurement of the neutron background at the Canfranc Underground Laboratory LSC

D. Jordan [a,*], J.L. Tain [a], A. Algora [a,1], J. Agramunt [a], C. Domingo-Pardo [a], M.B. Gomez-Hornillos [b], R. Caballero-Folch [b], G. Cortés [b], D. Cano-Ott [c], E. Mendoza [c], I. Bandac [d], A. Bettini [d,e], L.M. Fraile [f], C. Domingo [g]

[a] Instituto de Física Corpuscular, CSIC – Univ. Valencia, Valencia, Spain
[b] Universitat Politecnica de Catalunya, Barcelona, Spain
[c] Centro de Investigaciones Energeticas Medioambientales y Technologicas, Madrid, Spain
[d] Laboratorio Subterraneo de Canfranc, Canfranc Estacion, Spain
[e] Università di Padova and INFN, Padova, Italy
[f] Grupo de Física Nuclear, Facultad de Ciencias Físicas, Universidad Complutense de Madrid, Madrid, Spain
[g] Universitat Autonoma de Barcelona, Bellaterra, Spain

ARTICLE INFO

Article history:
Received 2 August 2012
Received in revised form 23 October 2012
Accepted 15 November 2012
Available online 25 November 2012

Keywords:
Neutron background
Underground physics
^{3}He proportional counters

ABSTRACT

The energy distribution of the neutron background was measured for the first time at Hall A of the Canfranc Underground Laboratory. For this purpose we used a novel approach based on the combination of the information obtained with six large high-pressure ^{3}He proportional counters embedded in individual polyethylene blocks of different size. In this way not only the integral value but also the flux distribution as a function of neutron energy was determined in the range from 1 eV to 10 MeV. This information is of importance because different underground experiments show different neutron background energy dependence. The high sensitivity of the setup allowed to measure a neutron flux level which is about four orders of magnitude smaller that the neutron background at sea level. The integral value obtained is $\Phi_{\text{Hall A}} = (3.44 \pm 0.35) \times 10^{-6}$ cm^{-2} s^{-1}.

1. Introduction

Deep underground laboratories provide a low radioactive background environment that is suitable for a large set of experiments aiming at very low count rate. These include astroparticle physics and nuclear astrophysics experiments, but also biological and geological studies. Specifically the large reduction of the cosmic ray muon flux compared to that at surface laboratories is of great advantage for rare event searches, otherwise hampered by muon-induced background at the surface. A further advantage of the use of underground laboratories for physics experiments is the reduction of the neutron background (in part muon induced) by several orders of magnitude with respect to sea level ($\Phi_{\text{sea}} \approx 10^{-2}$ cm^{-2} s^{-1}). The neutron background is a limiting factor in many rare event experiments because of the large penetrability of neutrons and the possibility of inducing background signals in the detection system. A precise determination of the background is therefore important in order to design shielding strategies and quantify sensitivity limits or systematic corrections. Given its importance for all the underground experiments, the neutron field has been measured with a number of techniques and in different energy ranges in the majority of the underground science laboratories [1]. In general these measurements provide the neutron flux integrated over wide neutron energy intervals. However in view of the strong energy dependence of the different neutron interaction mechanisms, with varying impact on the different underground experiments, it is extremely important to know the energy distribution of the neutron flux.

In experiments aiming at the direct detection of neutral Weak Interacting Massive Particles (WIMPs) by the induced nuclear recoils, neutrons can easily mimic their interaction and become the most dangerous source of experimental background [2–5]. Antineutrino detection experiments using the inverse β-decay reaction $\bar{\nu}_e + p \rightarrow n + e^+$ and aiming at the detection of the neutron also suffer from the presence of background neutrons. A similar problem occurs in other neutrino experiments based on the breakup of deuterium and the subsequent detection of the neutron [6]. Neutrons can produce also γ-rays through inelastic scattering and, after velocity moderation, through radiative capture. This radiation constitutes a background for experiments using γ-ray sensitive detectors [7].

* Corresponding author. Address: Instituto de Física Corpuscular, Apdo. Correos 22085, E-46071 Valencia, Spain. Tel.: +34 963543501; fax: +34 963543488.
E-mail address: jordan@ific.uv.es (D. Jordan).
[1] On leave from Institute of Nuclear Research, Debrecen, Hungary.

0927-6505/$ - see front matter © 2012 Elsevier B.V. All rights reserved.
http://dx.doi.org/10.1016/j.astropartphys.2012.11.007

At the Canfranc Underground Laboratory (LSC) several experiments under construction or being planned, from dark matter searches to nuclear astrophysics reaction cross-section measurements, require a good knowledge of the neutron background. In fact in the course of the preparation of the IGEX-DM experiment the neutron background has been already investigated [8] at the old LAB2500 of LSC. A value of $\Phi_{LAB2500} = 3.82(44)\times 10^{-6}$ cm^{-2} s^{-1} was estimated, due essentially to radioactivity-related neutrons coming from the rock. This number was obtained from a comparison of the low energy part of the spectrum registered in the HPGe detector with Monte Carlo (MC) simulations of assumed neutron fields. The method is sensitive to neutron energies above 10–100 keV. The muon-induced neutron component has been obtained in the aforementioned work to contribute only to the level of 10^{-9} cm^{-2} s^{-1}, almost three orders of magnitude lower than the neutron flux due to the rock radioactivity.

In our case, we are concerned with the possibility of carrying out measurements of (α,n) reaction cross-sections of astrophysical interest down to values of 1 pb or lower by direct detection of the outgoing neutron. Such reactions are a key ingredient of the scientific program of the CUNA project at LSC [9]. In particular the measurement of ^{22}Ne (α,n) [10]) and ^{13}C (α,n) reactions down to the lowest possible energies is the main goal of the project. These reactions are believed to be the source of neutrons for the slow neutron capture process (*s* process) leading to the formation of about half of the elements in the Universe beyond iron [11]. Neutron background represents a limiting factor for such measurements at sea level [12] hence the need for going underground. Both the design of the experiment and the evaluation of the expected detection limits require a good knowledge of the neutron flux energy distribution.

The challenge here is the measurement of the background neutron field at the expected very low rates. The detection system to be employed should have large neutron efficiency, large neutron discriminating capability, long term gain stability and a low rate of unwanted signals. The most popular device to measure neutron fields in dosimetry is the so-called Bonner Sphere Spectrometer (BSS) [13]. It consists of a small thermal neutron detector surrounded by neutron energy moderator spheres of different thicknesses. Neutrons of different energies have diverse detection efficiencies depending on the thickness of the moderating sphere. Combining the information of each of the spheres it is possible to deduce the absolute value and spectral shape of the neutron flux in the range of thermal energies up to tens of MeV. High-density polyethylene (PE) is normally used as the hydrogenated moderation material. Several options exist for the neutron detector, but a popular choice is a small gas proportional chamber filled with ^{3}He. Thermal neutrons have a large capture probability on helium-3, leading to the reaction: $^3\mathrm{He} + n \rightarrow {}^3\mathrm{H} + p$, with a positive *Q*-value of 764 keV. This reaction produces a well-isolated signal in the counter. Additionally, such type of detector is known to be relatively insensitive (as compared to other neutron detectors) to gamma-rays which could interfere the measurement. However, such BSS would have a disadvantage for our purpose, namely the limited efficiency due to the small detector size.

Our idea was to overcome the limitation of conventional BSS by using large high-pressure ^{3}He proportional tubes. Preliminary MC simulations showed that an increase in efficiency of two orders of magnitude could be readily obtained when compared versus the standard BSS detectors. We should point out that a similar measurement was carried out in the eighties at the Laboratori Nazionali del Gran Sasso but using BF_3 counters [14] instead of ^{3}He counters.

The use of large ^{3}He counters embedded in PE moderators has another advantage for our purposes. Among the different methods of detection employed to measure low (α,n) reaction cross sections above ground, a popular one has been the use of 4π neutron counters based on arrays of ^{3}He tubes embedded in large PE matrices [12,15]. In our opinion such a device is possibly the best candidate for measurements underground with high detection sensitivity. Therefore our setup provides also very valuable information concerning rates, stability, noise and additional background sources, for the future CUNA neutron detector.

This document reports on the first direct measurements, the analysis and the results concerning the neutron background spectrum at LSC using such device.

2. Experimental apparatus

2.1. Detection setup

The measurement setup consisted of six large ^{3}He proportional tubes, each one embedded in a PE block of different thickness. The proportional tubes, fabricated by LND [16], are part of a neutron detector developed for the study of β-delayed neutron emitters of importance for nuclear structure, astrophysics and reactor technology [17]. The most relevant characteristics of the tubes are an effective volume corresponding to a diameter 2.54 cm and a length of 60 cm and a filling pressure of 20 atm.

For the measurement at LSC the optimal number of detectors and the size of the moderating volumes were determined by means of a series of MC simulations. In the latter, several neutron energies were selected in the range from 10 meV to 100 MeV. The simulations were performed with the code MCNPX [18], which is considered a standard for neutron simulations in this energy regime. As a result it was decided to use six detectors with PE blocks of sizes given in Table 1.

The set-up was positioned in the middle of Hall A (almost empty at the time of the measurement) on a light structure which hold the counters, one meter above ground. The counters were distributed in a fan-like arrangement in order to maximize the distance between them, while minimizing the length of the cable connecting the proportional tube to the preamplifier, situated at the center of the arrangement, for electronic noise reduction. A schematic picture of the experimental setup is shown in Fig. 1.

2.2. Electronics and data acquisition

An schematic drawing of the electronic connections is shown in Fig. 2. Each proportional counter was connected to one of the inputs of the MPR16-HV Preamplifier from Mesytec [19]. A single HV module connected to the preamplifier powers all the counters connected to it. The differential output of the preamplifier was connected to a STM16 + Shaping Amplifier from Mesytec. The output of the amplifier was sent to the waveform digitizer of the data acquisition system (DACQ). A fix low frequency (10 Hz) pulse generator was connected to the test input of the preamplifier to determine the measuring time (acquisition live time).

A self-triggered DACQ developed originally for nuclear decay experiments [20] was employed to acquire the information from the detectors. The DACQ is based on the SIS3302 VME module, a 100 MHz 16-bit sampling digitizer from Struck Innovative Systems with Gamma Firmware [21]. Every signal in an ADC channel above a

Table 1
Dimensions of the neutron moderating polyethylene blocks.

Detector No.	PE block size (cm^3)
1	$4.5 \times 4.5 \times 70.0$
2	$7.0 \times 7.0 \times 70.0$
3	$12.0 \times 12.0 \times 70.0$
4	$18.0 \times 18.0 \times 70.0$
5	$22.5 \times 22.5 \times 70.0$
6	$27.0 \times 27.0 \times 70.0$

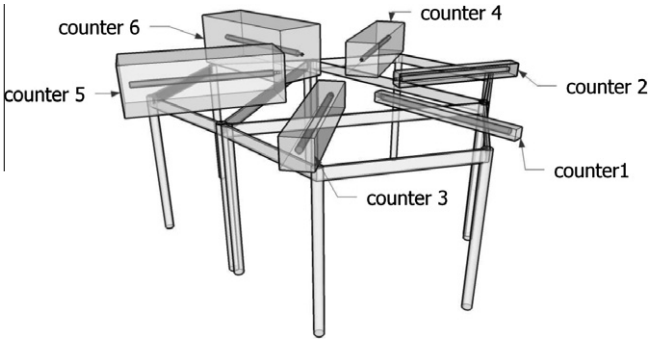

Fig. 1. View of the arrangement of the six detector modules: ^{3}He tube inside a polyethylene block.

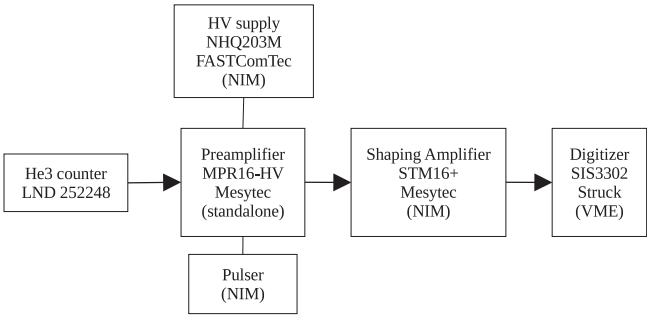

Fig. 2. Sketch of the electronic chain.

predefined threshold in the fast trapezoidal filter provides a time mark (in 10 ns steps with a range of 48 bits) and starts the energy filter that provides the signal amplitude. The ADC threshold was determined independently for each counter, in such a way that some amount of electronic noise was registered by the system (see Fig. 3). Module control and data transfer to a PC is carried out via the Struck SIS1100/3100 PCI/VME interface. Each channel stores the time–amplitude data pairs into a 64 MB memory. The memory space is divided into two data banks which are working in alternating mode: while one data bank is filled with the incoming data, the other one is being read-out through the VME bus. In this way a system with minimum dead time is achieved. The software, developed at IFIC-Valencia, allows the configuration and control of the system and performs the online analysis and visualization of the data.

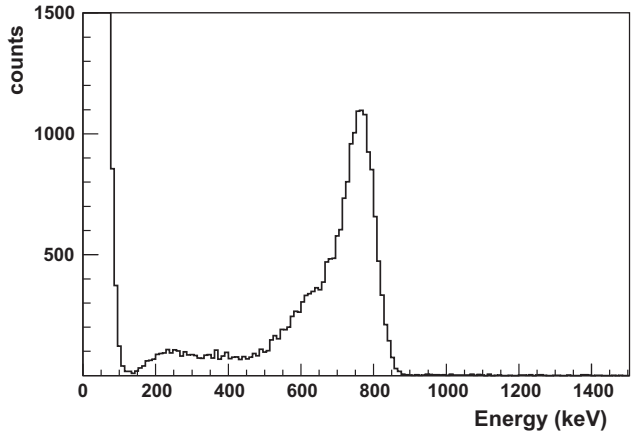

Fig. 3. Spectrum recorded in one of the detectors with the ^{252}Cf source. Signals below 100 keV correspond to noise.

3. Measurements

Before starting the neutron background measurement at Hall A, an efficiency calibration of each counter was performed placing a 400 n/s ^{252}Cf source on top of each detector. The uncertainty in the activity of the source was 10%. The main purpose of this measurement was to verify the accuracy of the MC simulation of the set-up, in particular the correctness of the geometrical description of the detector. The same simulation package is used to calculate the efficiency versus energy response matrix of the assembly that is needed in the analysis of the neutron background data.

Fig. 3 shows the spectrum recorded in one of the detectors with the ^{252}Cf source. The characteristic response of ^{3}He proportional counters to very low energy neutrons is visible. The peak at 764 keV corresponds to the full absorption of the proton and triton energy in the gas. The tail to the left is due to the partial energy absorption for one of the two particles when the break-up reaction occurs close enough to the inner-wall of the counter. The lower edge at 191 keV occurs when no energy is deposited by the proton, while the edge at 573 keV occurs when no energy is deposited by the triton. Notice the clear separation of neutron signals from electronic noise, concentrated below 100 keV, and the very small number of counts registered above 900 keV. The experimental efficiency is determined from the integral number of counts in the region 100–900 keV. The values are given in Table 2. The quoted uncertainty includes both the statistical uncertainty and the systematic uncertainty in the activity of the source which dominates the result.

The MC simulations were performed with the MCNPX code. The MC calculated efficiency is given in Table 2. The quoted uncertainty is due to the event statistics of the simulation. As it can be seen in Table 2 an excellent agreement between measurement and simulation is reached. This was only possible after including in the simulation a detailed geometrical description of the counter and of the source (1 cm^3 liquid solution in a thick plastic vial). In spite of the good agreement, the uncertainty in the source activity sets the limit in the uncertainty on the absolute value of the calculated efficiencies, which accordingly we set to 10%.

The neutron background measurement at the Hall A of LSC lasted 26 days. In the off-line analysis it was observed that some of the counters became very noisy for (very) short periods of time and the corresponding data was excluded from the analysis. The total accumulated spectra for the six counters can be seen in Fig. 4.

In all spectra one can clearly distinguish counts in the region between 150 and 900 keV, which are associated with neutron detection events. It is also clear that these signals are superposed to other background signals whose relative importance changes for the different detectors. However, it is possible to disentangle the different contributions using the neutron response measured with the ^{252}Cf source and a linear function to fit the region between 700 and 1500 keV as it is shown in the figure. The major component of the remaining background counts is concentrated between 100 and 600 keV. It is not totally clear at present the origin of these additional background contributions. One could speculate that the low energy component is due to γ-rays and eventually β-particles

Table 2
Comparison of experimental and simulated efficiency for the ^{252}Cf calibration source.

Detector No.	Experiment eff. (%)	MCNPX eff. (%)
1	0.33 (3)	0.37 (2)
2	1.44 (14)	1.39 (4)
3	2.36 (24)	2.19 (5)
4	1.52 (15)	1.55 (4)
5	0.91 (9)	0.92 (3)
6	0.52 (5)	0.53 (2)

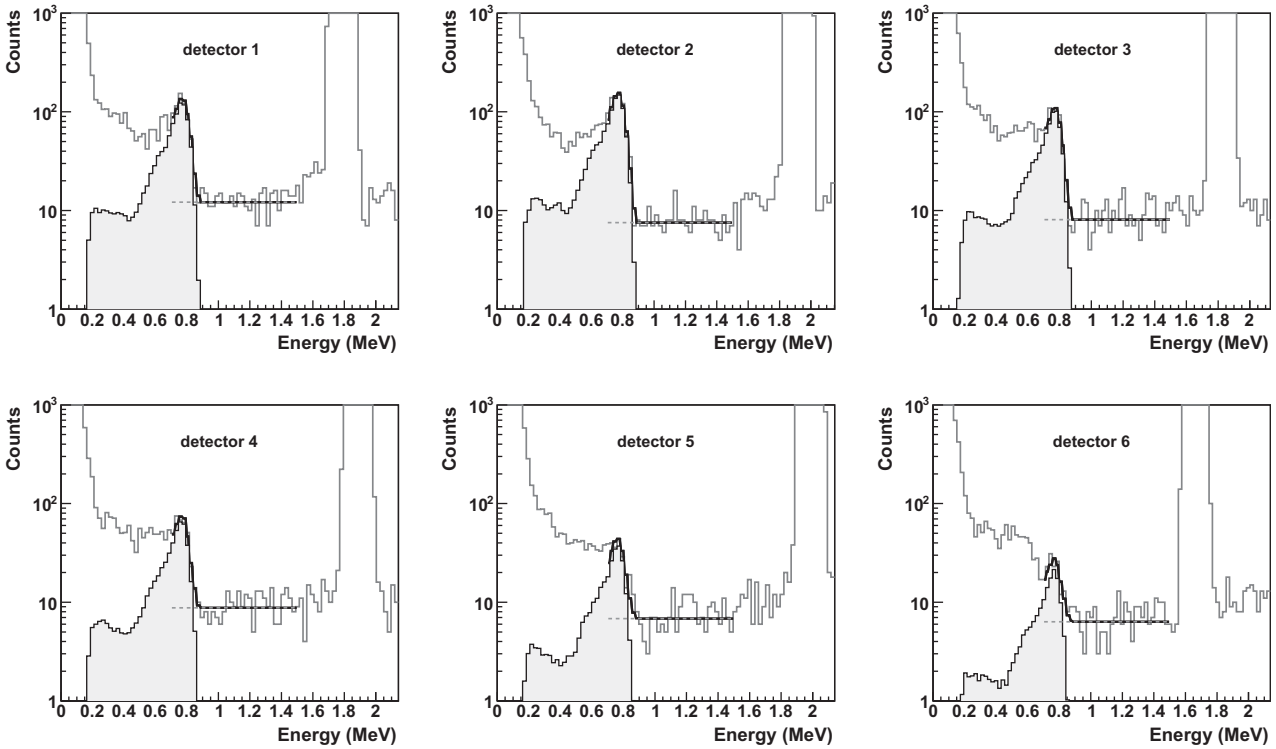

Fig. 4. Spectra accumulated during 26 days for all six detectors. The peak below 100 keV corresponds to electronic noise and the peak at 1.8 MeV corresponds to the pulse generator. The filled gray histogram represents the neutron response and the gray dashed line represents a high-energy linear background. The black histogram represents the fit.

Table 3
Neutron background rate measured at LSC with the different counters.

Detector No.	Neutron rate (s^{-1})
1	$4.38\ (20) \times 10^{-4}$
2	$5.04\ (21) \times 10^{-4}$
3	$3.79\ (19) \times 10^{-4}$
4	$2.33\ (16) \times 10^{-4}$
5	$1.28\ (12) \times 10^{-4}$
6	$7.70\ (97) \times 10^{-4}$

coming from residual radioactivity in the counter materials. On the other hand, there is enough previous information [22] to conclude that the high-energy background component is due to α-radioactivity coming from the counter walls. This should be further investigated and in particular the possibility of reducing these additional background components with the prospect of using this type of detector for the measurement of neutron producing reaction cross-sections of astrophysical interest at LSC.

4. Data analysis

From the area of the histogram representing the neutron counts and the area of the pulse generator peak located around 1.8 MeV (measuring time) in Fig. 4 we can determine the neutron background rate for each detector. The result is given in Table 3. The quoted uncertainty (one sigma), ranging between 4% and 13%, is coming from the uncertainty in the area fit parameter. The chosen fit region (700–1500 keV) produces the best fit results, with reduced chi square values ranging from 0.8 to 1.3.

The count rate in each detector C_i is related to the neutron flux energy distribution Φ_j through the efficiency versus energy response matrix R_{ij}:

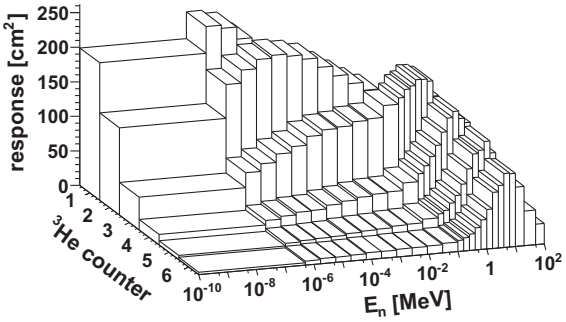

Fig. 5. Detector versus neutron energy response matrix.

$$C_i = \sum_j R_{ij}\Phi_j \tag{1}$$

The response matrix R_{ij} relates the counts registered in detector labeled i with the number of neutrons with energy labeled j. The response matrix is obtained by MC simulation with the simulation package validated by the calibration measurement. Neutron energies range from 10^{-10} to 100 MeV. This energy interval is distributed into 24 energy bins. The first bin covers the thermal peak. The range between 5×10^{-7} and 0.1 MeV is distributed in ten logarithmic bins. Ten additional logarithmic bins cover the next range up to 10 MeV. The next three bins reach 20, 50 and 100 MeV respectively. In the simulation, neutron energies are randomly sampled within each bin. Neutrons are assumed to fall isotropically on all surfaces of the PE block. The area of the PE block surface is used to scale the result of the simulation in order to obtain the proper normalization. Fig. 5 shows the calculated response function for each detector (in units of cm^2) as a function of the energy bin. It can be appreciated that the peak of the response function

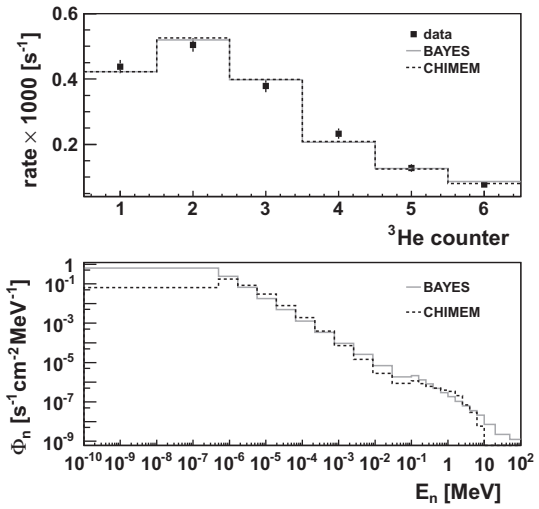

Fig. 6. Upper panel: reconstructed counting rate compared with data. In gray the result of the BAYES code and the dashed black line corresponds to the result of CHIMEM code. Lower panel: neutron flux obtained using the two codes.

moves to higher energies as the PE volume dimension increases. If we compare the scale of Fig. 5 with the scale of Fig. 1 of Ref. [23], the large increase in efficiency for our setup in comparison with conventional BSS using a small volume neutron detector becomes patent.

In order to obtain the neutron flux distribution Φ_j we must solve the linear inverse problem represented by Eq. (1). It belongs to the class of ill-posed (ill-conditioned) inverse problems for which a variety of methods of solution have been developed [24]. The solution Φ_j of the problem represented by Eq. (1) is not unique since is one that reproduces the data C_i within the experimental uncertainties. Therefore different codes produce different solutions depending on the method of solution, the adjustable parameters of the method, or computer numerical round-off errors. It is generally recognized that the best way to investigate this type of systematic uncertainty is to apply different codes and compare the results.

We have chosen to use two different codes which were originally developed [25] to analyze spectra obtained in β-decay total absorption spectroscopy experiments, but which otherwise are based on commonly employed inversion methods. The code BAYES is based on the Expectation–Maximization method while the code CHIMEM is based on the Maximum Entropy method. Both algorithms are iterative and require a starting guess solution and a stopping criterion. The code CHIMEM requires also a regularization parameter but it has been found that the solution depends little on its value if convergence is obtained. In the present case we have chosen a flat flux distribution as initial guess and the stopping criterion was set to obtain a reduced chi-square χ^2/ν between the experimental data and the reconstructed data close to unity.

The reconstructed counting rate obtained using the two different algorithms is compared with the experimental counting rate in the upper panel of Fig. 6. As it can be observed the difference between both methods is very small, practically indistinguishable in the figure. Differences are larger with the experimental rates although in both cases the value of χ^2/ν is close to one. The deduced neutron flux has been plotted in the lower panel of Fig. 6. The flux values and uncertainties are given in Table 4 for every energy bin. The quoted flux uncertainty is due solely to the uncertainty in the rates and is calculated by error propagation (see Ref. [25] for details). Since this uncertainty is quite small (2.5–5%) it does not show up in the lower panel of Fig. 6. The shape of both flux distributions is very similar although large differences can be observed for particular energy bins. This is the case for thermal energies, for energies around 10–100 keV and for energies above 10 MeV. In spite of this differences the integral value of the flux obtained with both codes differs by less than 10%: $\Phi_{\text{BAYES}} = 3.61(8) \times 10^{-6}$ cm^{-2} s^{-1} and $\Phi_{\text{CHIMEM}} = 3.31(9) \times 10^{-6}$ cm^{-2} s^{-1}. The quoted error was obtained using the full covariance matrix calculated by the codes.

Table 4
Flux values and uncertainties for every energy bin.

Energy bin (MeV)		Φ (cm^{-2} s^{-1} MeV^{-1})			
Lower limit	Upper limit	BAYES	CHIMEM	GRAVEL	MAXED
1.00×10^{-10}	5.00×10^{-7}	0.64 (2)	$6.45\ (15) \times 10^{-2}$	1.12	0.01
5.00×10^{-7}	1.69×10^{-6}	0.24 (1)	0.18 (1)	0.22	0.14
1.69×10^{-6}	5.74×10^{-6}	$6.68\ (17) \times 10^{-2}$	$8.49\ (26) \times 10^{-2}$	0.06	0.11
5.74×10^{-6}	1.95×10^{-5}	$1.81\ (5) \times 10^{-2}$	$3.04\ (9) \times 10^{-2}$	0.02	0.04
1.95×10^{-5}	6.60×10^{-5}	$4.85\ (12) \times 10^{-3}$	$7.86\ (24) \times 10^{-3}$	3.90×10^{-3}	7.02×10^{-3}
6.60×10^{-5}	2.24×10^{-4}	$1.29\ (3) \times 10^{-3}$	$1.91\ (5) \times 10^{-3}$	8.32×10^{-4}	1.06×10^{-3}
2.24×10^{-4}	7.58×10^{-4}	$3.46\ (8) \times 10^{-4}$	$4.00\ (11) \times 10^{-4}$	2.20×10^{-4}	1.98×10^{-4}
7.58×10^{-4}	2.57×10^{-3}	$9.44\ (22) \times 10^{-5}$	$7.24\ (19) \times 10^{-5}$	7.33×10^{-5}	4.18×10^{-5}
2.57×10^{-3}	8.71×10^{-3}	$2.58\ (6) \times 10^{-5}$	$1.45\ (4) \times 10^{-5}$	2.72×10^{-5}	1.17×10^{-5}
8.71×10^{-3}	2.95×10^{-2}	$7.01\ (17) \times 10^{-6}$	$2.78\ (6) \times 10^{-6}$	8.66×10^{-6}	3.16×10^{-6}
2.95×10^{-2}	0.10	$1.90\ (5) \times 10^{-6}$	$8.76\ (21) \times 10^{-7}$	3.05×10^{-6}	1.38×10^{-6}
0.10	0.16	$2.18\ (5) \times 10^{-6}$	$1.16\ (3) \times 10^{-6}$	1.65×10^{-6}	1.04×10^{-6}
0.16	0.25	$1.32\ (3) \times 10^{-6}$	$8.46\ (22) \times 10^{-7}$	1.08×10^{-6}	7.52×10^{-7}
0.25	0.40	$8.13\ (2) \times 10^{-7}$	$6.17\ (16) \times 10^{-7}$	9.79×10^{-7}	8.63×10^{-7}
0.40	0.63	$4.88\ (14) \times 10^{-7}$	$4.94\ (14) \times 10^{-7}$	5.51×10^{-7}	5.57×10^{-7}
0.63	1.00	$3.00\ (9) \times 10^{-7}$	$3.93\ (12) \times 10^{-7}$	3.93×10^{-7}	5.92×10^{-7}
1.00	1.58	$1.83\ (6) \times 10^{-7}$	$3.37\ (11) \times 10^{-7}$	2.54×10^{-7}	6.12×10^{-7}
1.58	2.51	$1.07\ (4) \times 10^{-7}$	$2.10\ (7) \times 10^{-7}$	9.74×10^{-8}	1.42×10^{-7}
2.51	3.98	$6.26\ (23) \times 10^{-8}$	$7.06\ (26) \times 10^{-8}$	4.48×10^{-8}	3.23×10^{-8}
3.98	6.31	$3.63\ (15) \times 10^{-8}$	$2.91\ (11) \times 10^{-8}$	2.08×10^{-8}	7.21×10^{-9}
6.31	10	$2.11\ (9) \times 10^{-8}$	$5.91\ (20) \times 10^{-9}$	9.51×10^{-9}	1.50×10^{-9}
10	20	$7.25\ (33) \times 10^{-9}$	$4.17\ (10) \times 10^{-10}$	6.01×10^{-9}	8.91×10^{-10}
20	50	$2.23\ (11) \times 10^{-9}$	$2.08\ (3) \times 10^{-11}$	3.63×10^{-9}	2.65×10^{-9}
50	100	$1.23\ (6) \times 10^{-9}$	$4.71\ (4) \times 10^{-12}$	0.00	0.00

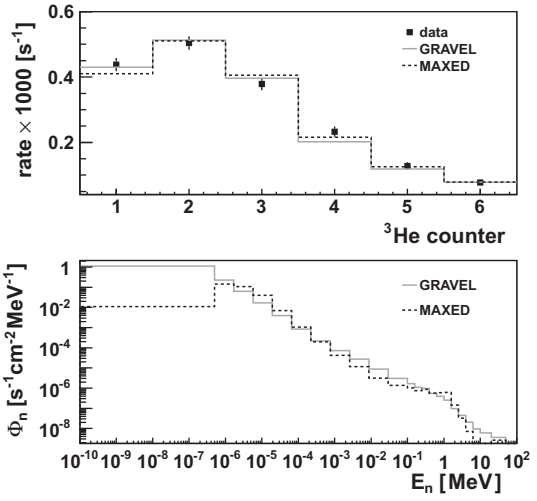

Fig. 7. Same as Fig. 6. In gray the result of the GRAVEL code and the black dashed line corresponds to the result of MAXED code.

In order to further confirm the results, we decided to analyze the data with two standard codes that are used in the analysis of BSS data: MAXED [26] based on the Maximum Entropy principle and GRAVEL (based on a modified version of SAND-II code) [27], a non-linear least squares minimization algorithm. Both are distributed by the Nuclear Energy Agency as part of the package UMG.

The results obtained are shown in Fig. 7. As it can be observed, a comparable reproduction of the data is obtained and the general shape of the flux distribution is similar for both codes. Moreover, the results are close to the ones presented in Fig. 6 as can be verified in Table 4 where the flux values per bin are given. The largest differences between both flux distributions are found in the same energy regions as in Fig. 6. The integral value of the flux is $\Phi_{GRAVEL} = 3.61 \times 10^{-6}$ cm^{-2} s^{-1} and $\Phi_{MAXED} = 3.32 \times 10^{-6}$ cm^{-2} s^{-1} respectively, very similar to the values found above. No error was calculated by the codes in this case.

The large differences observed between the four flux distributions at thermal energies (first bin) and above 10 MeV, actually reflect that our setup has a limited sensitivity at those energies. This can be seen in the response matrix depicted in Fig. 5, where none of the detectors has a maximum for thermal energies or at high energies. We plan to enhance the sensitivity for thermal energies adding a bare counter to the setup, and the sensitivity at high energies including detectors which combine the PE layers with layers of material having large (n,Xn) cross sections that acts as a high energy neutron converter-multiplier. However this requires to have access to several installations with well characterized neutron beams at these energies in order to perform the efficiency calibration and we preferred to restrict the present setup to those detectors that we could calibrate properly with the ^{252}Cf source.

We can calculate the weighted average of the integral flux values in order to obtain the flux in the center of Hall A at LSC. The calculated uncertainty (less than 2%) reflects the statistical uncertainty in the data. To this we have to add the 10% systematic uncertainty coming from the efficiency calibration, which dominates the result:

$$\Phi_{\text{Hall A}} = (3.44 \pm 0.35) \times 10^{-6}\ \text{cm}^{-2}\ \text{s}^{-1}$$

Notice that the maximum difference between the values obtained with the four codes is 9%. This difference is related to the additional systematic uncertainty due to the inversion code.

The integral of the flux distribution that we obtain above 10 keV is about 1.4×10^{-6} cm^{-2} s^{-1}. This value can be compared with the one quoted in [8] (see also Section 1) for LAB2500 of LSC, being a factor (close to) three lower. Above 10 keV the flux is dominated by rock radioactivity: i.e. fission neutrons from U and (α,n) reactions induced by the alpha radioactivity of Th–U decay chains on light elements. These components have maximum contributions at neutron energies around 0.6 and 3.5 MeV respectively. The differences between both measurements can be explained by a different rock composition at both sites, the thicker concrete layer on the walls at Hall A and the much smaller distance of the detector to the walls at LAB2500.

5. Conclusion

We have measured the neutron background flux in the center of Hall A of LSC to be $\Phi_{\text{Hall A}} = (3.44 \pm 0.35) \times 10^{-6}$ cm^{-2} s^{-1}. For this we used six large high-pressure ^{3}He proportional counters, each one embedded in a polyethylene neutron moderation block of different size in a manner analogous to a Bonner Sphere Spectrometer. The flux distribution as a function of neutron energy was also well determined in the range of 1 eV–10 MeV.

We have shown that this type of device can be applied successfully to the measurement of very low neutron levels, which are four orders of magnitude smaller than the ambient background at sea level. The demonstrated high sensitivity of the setup is also of importance in view of the planned measurements of very low (α,n) cross-sections of astrophysical interest using 4π neutron counters based on ^{3}He proportional tubes, which are part of the scientific program of the CUNA project.

Acknowledgments

This work was supported by the Spanish Ministerio de Economía y Competitividad under Grants CONSOLIDER-Ingenio 2010 CSD2008-0037 (CUP), FPA2011-28770-C03-03, FPA2011-24553, FPA2010-17142 and CSD-2007-00042 (CPAN). The authors want to acknowledge the help of the LSC personnel in the preparation and execution of the measurements.

References

[1] A. Bettini, Nucl. Instrum. Methods A 626 (2011) S64.
[2] V. Chazal et al., Astropart. Phys. 9 (1998) 163.
[3] H.J. Kim et al., Astropart. Phys. 20 (2004) 549.
[4] H. Wulandari et al., Astropart. Phys. 22 (2004) 313.
[5] E. Tziaferi et al., Astropart. Phys. 27 (2007) 326.
[6] J.F. Amsbaugh et al., Nucl. Instrum. Methods A 579 (2007) 1054.
[7] Ch. Marquet et al., Nucl. Instrum. Methods A 457 (2001) 487.
[8] J.M. Carmona et al., Astropart. Phys. 21 (2004) 523.
[9] L.M. Fraile et al., Canfrac underground nuclear astrophysics facility (CUNA), Status Report, November 2011.
[10] R. Longland et al., Reaction rates for the *s*-process neutron, Source 22Ne+a, <arXiv:1206.3871v1>.
[11] F. Kaeppeler et al., Rev. Mod. Phys. 83 (2011) 157.
[12] M. Jaegger et al., Phys. Rev. Lett. 87 (2001) 202501.
[13] R.L. Bramblett et al., Nucl. Instrum. Methods 9 (1960) 1.
[14] P. Belli et al., Il Nuovo Cimento 101A (1989) 959.
[15] H.W. Drotleff et al., Astrophys. J. 414 (1993) 735.
[16] <http://www.lndinc.com/>.
[17] M.B. Gomez-Hornillos et al., J. Phys. Conf. Ser. 312 (2011) 052008.
[18] D. Pelowitz (Ed.), MCNPX Users Manual Version 2.5.0, Los Alamos National Laboratory, Report LA-CP-05-0369, April 2005.
[19] <http://www.mesytec.com/>.
[20] J. Agramunt, Master Thesis, University of Valencia, in preparation.
[21] <http://www.struck.de/>.
[22] J.F. Amsbaugh et al., Nucl. Instrum. Methods A579 (2007) 1054.
[23] D.J. Thomas et al., Nucl. Instrum. Methods A476 (2002) 12.
[24] Albert Tarantola, Inverse Problem Theory: Methods for Data Fitting and Model Parameter Estimation, Elsevier, New York, 1987.
[25] J.L. Tain, D. Cano, Nucl. Instrum. Methods A571 (2007) 728.
[26] M. Reginatto et al., Nucl. Instrum. Methods A476 (2002) 242.
[27] M. Matzke, Rad. Prod. Dosim. 107 (2003) 155.